Icarus 226 (2013) 20–32

Contents lists available at SciVerse ScienceDirect

Icarus

journal homepage: www.elsevier.com/locate/icarus

Dynamics of core merging after a mega-impact with applications to Mars' early dynamo

J. Monteux [a,b,*], A.M. Jellinek [b], C.L. Johnson [b,c]

[a] Laboratoire de Planétologie et de Géodynamique de Nantes, UMR CNRS, Université de Nantes, France
[b] Department of Earth, Ocean and Atmospheric Sciences, University of British Columbia, Canada
[c] Planetary Science Institute, Tucson, AZ, United States

ARTICLE INFO

Article history:
Received 3 October 2012
Revised 23 April 2013
Accepted 9 May 2013
Available online 18 May 2013

Keywords:
Mars, Interior
Magnetic fields
Impact processes
Planetary dynamics

ABSTRACT

A giant impact occurring within the first 500 Myr of martian history may have been responsible for the dichotomy between the northern lowlands and the southern highlands and may have influenced the initiation or cessation of early and short-lived core dynamo. We hypothesize that a significant volume of metallic iron from a differentiated impactor merged with a preexisting martian core. We investigate the dynamics and thermal effects of this core merging, assuming that the impactor's core sank as a single metallic diapir through a solid mantle. We explore the consequences of this process for dynamo action and for Mars' magnetic field history. For large impacts (with radii larger than 100 km) and plausible mantle viscosities, merging is expected to occur in less than 1 Myr. Depending on the temperature-dependence of the mantle viscosity, viscous dissipation within the diapir may be very large. Where thermal mixing of the hot diapir into a preexisting core is complete, merging can increase the temperature gradient to the surrounding mantle and consequently drive a dynamo until this additional heat is transferred to the mantle, which takes on the order of 100 Myr. If merging leads to strong thermal stratification in the core, however, dynamo action may be inhibited.

1. Introduction

Mega impacts (with an impactor/target radius ratio between one tenth and 1) probably played an important role in the late history of terrestrial planetary accretion. An impact between the proto-Earth and a Mars-size protoplanet can, for example, explain the Earth–Moon system (Hartmann and Davis, 1975) and a large impact removing part of the silicate mantle is a hypothesis for the high iron/silicate ratio on Mercury (Smith, 1979; Benz et al., 1988). Among the hypotheses for the origin of the martian dichotomy including an endogenic origin (Elkins-Tanton et al., 2003; Roberts and Zhong, 2006; Citron and Zhong, 2012) or a plate-tectonics feature (Sleep, 1994), an exogenic origin by a mega impact that displaced crustal material from the northern to the southern hemisphere seems to be the most plausible candidate (Wilhelms and Squyres, 1984; Nimmo et al., 2008; Andrews-Hanna et al., 2008; Marinova et al., 2008, 2011). Models for the martian impact suggest that the impactor was 800–1300 km in radius and hit the planet with a speed comparable to or larger than the martian escape velocity (i.e. $v_{imp} > 5$ km s^{-1}) within the first 500 Myr of martian history (Frey, 2006). Such a dramatic event can generate a debris disk around Mars that could have re-accreted and formed the martian moons (Rosenblatt, 2011).

In addition to a history of large impacts, Earth, Mercury and Mars have, or have had, an internally generated magnetic field. Mercury and the Earth have active core dynamos, whereas widespread crustal magnetism strongly suggest that Mars had an early internally-generated magnetic field (Acuña et al., 1999; Hood et al., 2003; Lillis et al., 2008a) that ceased by around 4.0 Ga (Acuña et al., 1999; Johnson and Phillips, 2005; Lillis et al., 2008b). The timing of the initiation of the martian dynamo is difficult to constrain and strongly depends on the differentiation processes that occurred during the first million years of martian history (Monteux et al., 2011). The cause of the cessation of the martian dynamo is also still currently debated. Recent models explore the effects of large impacts on the dynamo generation process, and in particular on the cessation of dynamo action as a result of a reduction of the core–mantle boundary (CMB) heat-flux (Roberts et al., 2009; Watters et al., 2009; Roberts and Arkani-Hamed, 2012). Shock heating within the core can also increase the CMB heat flow and create a thermal stratification that prevents heat loss from the inner part of the core, inhibiting core convection (Arkani-Hamed and Olson, 2010). Alternatively, other models show that the thermal anomaly induced by a large impact and the formation of a hot molten iron layer from the impactor's core at the CMB can favor dynamo generation (Reese and Solomatov, 2010).

* Corresponding author at: Laboratoire de Planétologie et de Géodynamique de Nantes, UMR CNRS, Université de Nantes, France.
E-mail address: julien.monteux@univ-nantes.fr (J. Monteux).

0019-1035/$ - see front matter © 2013 Elsevier Inc. All rights reserved.
http://dx.doi.org/10.1016/j.icarus.2013.05.008

At the time of the proposed giant impact, both Mars and the impactor were probably differentiated (Yoshino et al., 2003). Models suggest that although some material was ejected far from Mars, the majority of the mass of the impactor's core was retained within the planet and merged with the pre-impact martian core (Canup, 2004; Ćuk and Stewart, 2012). The aim of this study is to characterize the dynamics of core merging as a result of a diapiric descent of molten iron (Monteux et al., 2009) on a Mars-size planet. In addition, we investigate how the processes of impact and core merging might influence the thermal regime of Mars' core and, in turn, magnetic field generation (cf., Monteux et al., 2011).

2. Thermo-chemical state before the martian mega-impact

2.1. Pre-impact interior of Mars

The initial structure and thermal state of a growing planet is determined by the characteristics of its accretion from chondritic material (Safronov, 1978; Kaula, 1979; Agee, 1997). During accretion, heating driven by a combination of the dissipation of impact energy and the decay of short lived radionuclides such as ^{26}Al and/or ^{60}Fe (Yoshino et al., 2003; Monteux et al., 2007) increases the mean internal temperature and gives rise to a radial temperature gradient that depends on the accretion rate relative to the rate of radiative cooling to space (Kaula, 1979; Senshu et al., 2002). If the growth rate is very high in comparison to surface cooling, this heating can ultimately cause partial or complete melting of the chondritic material (Yoshino et al., 2003) and lead to extensive metal/silicate separation (Tonks and Melosh, 1992; Senshu et al., 2002; Monteux et al., 2009).

Hf/W chronology suggests that core formation happened during the first 10–30 myr of Mars' history (Lee and Halliday, 1997; Nimmo and Kleine, 2007). Such a rapid process involves extensive melting potentially enhanced by radiogenic heating as a result of the decay of short-lived radionuclides (Yoshino et al., 2003), impact heating (Tonks and Melosh, 1992; Senshu et al., 2002; Monteux et al., 2009) and gravitational energy conversion during metal/silicate separation (Stevenson, 1989; Ricard et al., 2009). Metal/silicate separation can occur via a wide range of phenomena such as percolation (Shannon and Agee, 1996), the sedimentation of metallic rain through a magma ocean (Rubie et al., 2003; Höink et al., 2005) or a large diapir sinking through a solid mantle after an impact (Tonks and Melosh, 1992; Monteux et al., 2009). Whatever the mechanism, Mars' internal structure characterized by a ~1700 km diameter Fe-core was mostly established within ~10 Myr of the planet's formation (Yoder et al., 2003) (cf., Fig. 1a).

The gravitational heat released during martian core formation was partitioned between the planet's core and mantle. The fraction of gravitational heat taken up by the metal or the silicate fraction depends strongly on the rheology of the planet and on the segregation mechanisms (Samuel and Tackley, 2008; Monteux et al., 2009; Ke and Solomatov, 2009). The combined processes leading to core formation yield a wide range of possible early thermal states, depending on the nature and timescale of the core formation process and the heat transfer properties of Mars' early mantle. In particular, the core could initially have had a temperature close to the deep mantle temperature if thermal equilibration was efficient. Alternatively, it could have been hotter than the mantle if the gravitational potential energy released during core formation was largely retained within the core itself, a situation which would lead to potentially strong cooling to the mantle (Fig. 1a).

2.2. Interior structure of the impactor

In this study, we consider impactors with a radius in the range 200–800 km. The lower bound for our range is motivated by the impactor size needed to create large impact basins such as Hellas or Utopia, and the upper bound is motivated by the minimum impactor radius needed in exogenic models for the dichotomy boundary (Marinova et al., 2008). Assuming that both the impactor and the target body had chondritic compositions, their volumetric metal fractions, f_0, should be similar (we consider that the impactor has the same metal content as Mars and we use $f_0 = 12.5\%$ (Stevenson, 2001)). Hence, for 200–1300 km diameter impactors, an additional volume of core material with a radius between 100 km and 700 km merges with the preexisting core (Fig. 1).

3. Thermo-chemical state after a mega-impact

3.1. Mantle heating and melting

Kinetic energy of the impactor is dissipated as a result of the irreversible work done by shock waves in damaging crustal rocks (Senshu et al., 2002; Monteux et al., 2011) as well as heating and melting the target material. This dissipation process is a complex mechanism that is still poorly constrained specially for giant impact events. In our models, we consider that post-impact heating and melting mostly occurs within a spherical region with a volume V_{ic} (and a radius R_{ic}) that is typically taken to be 3 times larger than the volume V_{imp} of the impactor itself (O'Keefe and Ahrens, 1977; Croft, 1982; Pierazzo et al., 1997). The energy available to heat and melt the target planet is $\Delta E = \gamma m_{imp} v_{imp}^2/2$, where γ is the fraction of the kinetic energy of the impactor ultimately dissipated to heat up the mantle (O'Keefe and Ahrens, 1977), m_{imp} is the impactor mass and v_{imp} is the impact velocity. The energy needed to melt a silicate volume V_{ic} is $\Delta E_{m,Si} = \rho_{Si} V_{ic} L_{Si}$, where ρ_{Si} and L_{Si} are the density and latent heat of the silicate material. The energy needed to melt the impactor core is $\Delta E_{m,Fe} = \rho_{Fe} f_0 V_{imp} L_{Fe}$ with L_{Fe} and ρ_{Fe} are the density and latent heat of the impactor's core.

In the heated region the temperature increases uniformly from an initial value T_0 by an amount ΔT_0 (Fig. 1c). The excess temperature ΔT_0 decreases rapidly and smoothly with distance r from the boundary of the isothermal anomaly as approximately $\Delta T_0 (R_{ic}/r)^m$ (Fig. 1c). Following Senshu et al. (2002), and fitting the decay of peak pressure with distance away from the edge of the isobaric core $m \approx 4.4$ (Monteux et al., 2007). The energy needed to increase the temperature inside and outside the isobaric core is $\Delta E_{th} = h_m \rho_{Si} V_{ic} C_{p,Si} \Delta T_0$, where $C_{p,Si}$ is the specific heat of the silicate material and h_m is a geometric parameter representing the amount of heat that is used to increase the temperature inside and outside the isobaric core relative to the amount of heat used to increase the temperature by ΔT_0 within the isobaric core (Senshu et al., 2002; Monteux et al., 2011) and

$$h_m = 1 + \frac{3(2m-5)}{2(m-3)(m-2)} \approx 2.7 \tag{1}$$

Hence, from the following energy balance:

$$\Delta E = \Delta E_{th} + \Delta E_{m,Si} + \Delta E_{m,Fe} \tag{2}$$

and using $m_{imp} = \rho_0 V_{imp} = \rho_0 V_{ic}/3$, we obtain:

$$\Delta T_0 = \frac{1/6 \gamma \rho_0 v_{imp}^2 - L_{Si}\rho_{Si} - f_0/3 L_{Fe}\rho_{Fe}}{h_m \rho_{Si} C_{p,Si}} \tag{3}$$

Assuming that the impact velocity is equal to the escape velocity of the planet we obtain a minimum estimate for the kinetic energy where $v_{imp} = v_{esc} = \sqrt{2gR}$ with $g = 4/3\pi G \rho_0 R$, G the gravitational constant and R the radius of the target planet. After some algebra:

$$\Delta T_0 = \frac{4/9\pi\gamma\rho_0^2 G R^2 - L_{Si}\rho_{Si} - \frac{f_0}{3} L_{Fe}\rho_{Fe}}{h_m \rho_{Si} C_{p,Si}}, \tag{4}$$

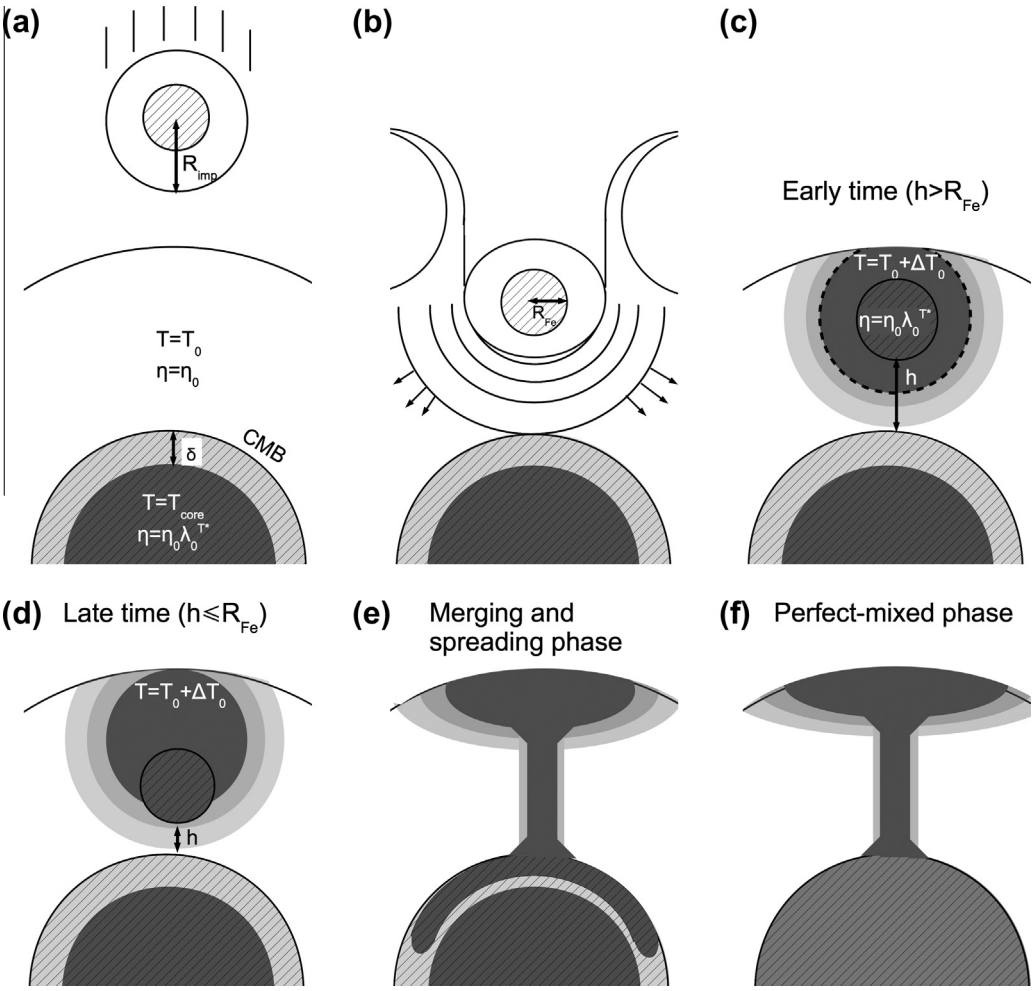

Fig. 1. Schematic representation of the thermo-chemical evolution following a mega-impact on a Mars-size body. After the impact (a) and the subsequent shockwave propagation (b), the impactor's core, radius R_{Fe}, is buried within the martian mantle and a large thermal anomaly remains (c). The post-impact temperature increase is constant within a volume delimited by the dashed line and rapidly decreases away from it. The dense metallic material from the impactor rapidly sinks towards the pre-impact martian core. During the sinking, potential energy is converted into heat in the mantle via viscous dissipation. Two sinking regimes occur (c and d) depending on the distance h between the impactor and the martian core (see Section 4). Finally the intruded metallic material merges with the preexisting core, spreads at its top (e) and eventually mixes with it later (f). The hatched volumes represent the metallic material from the martian core and the impactor. Gray shading represents temperature of the silicate (unhatched) or metallic (hatched) material and shows schematically the evolution of the thermal anomaly in the mantle during the sinking and merging phases (see also Fig. 5, left column).

For a Mars-sized planet with a mantle temperature close to its solidus the impact heating is always sufficiently large to completely melt the impacted mantle volume V_{ic} (i.e., $\Delta T_0 > 0$). For smaller or much colder planets, impact heating may only partially melt the impacted region, depending on the slope of the mantle solidus in temperature-composition space (Ernst et al., 2010; Roberts and Barnouin, 2012).

Noting that f_0 is O (10^{-1}), the term representing the energy needed to melt the impactor's core has a minor influence compared to the mantle melting term in Eq. (4). Hence, Eq. (4) can be simplified to give:

$$\Delta T_0 \approx \frac{4/9\pi\gamma\rho_0^2 GR^2 - L_{Si}\rho_{Si}}{h_m \rho_{Si} C_{p,Si}}, \tag{5}$$

Indeed using the set of parameters in Table 1 and making the assumption that the martian mantle before the impact is solid and close to its solidus, $\Delta T_0 \sim 400$ K. Including the impactor's core melting term in Eq. (4) would only reduce ΔT_0 by $\sim$10 K.

3.2. The fate of the impactor's material

During the mega-impact, a significant fraction of the impactor's silicate mantle is ejected far from the impact site to form a disk of debris, but most of the impactor's core is retained within the target planet (Canup, 2004; Ćuk and Stewart, 2012) (cf., Fig. 1b and c). For simplicity we assume that the full volume of the impactor's core is retained within the martian mantle after the giant impact. This assumption is reasonable for impact velocities close to the escape velocity of the target planet (Asphaug, 2010). We assume a solid mantle prior to impact, and that the impactor core sinks as a single, spherical diapir.

4. Dynamic models of diapir sinking

Once buried below the surface, the dense metallic core of the impactor sinks towards the center of the target planet (Fig. 1). Dissipation of the work done by buoyancy forces driving motion of this diapir occurs by a combination of viscous, viscoplastic (Samuel and Tackley, 2008), elasto-plastic (Gerya and Yuen, 2007) and fracturing (Davies, 1982; Stevenson, 2003) processes and causes heating in the mantle and/or the diapir, depending on the deformation regime. Where the effective mantle viscosity is very large in comparison to that of the diapir dissipation is concentrated in the mantle. As viscosity variations decline in response to heat transfer from the diapir to the mantle, however, dissipation will increasingly oc-

Table 1
Typical parameter values for numerical models.

Mars radius	R	3400 km
Mars core radius	R_c	1700 km
Thickness of the core thermal boundary layer	δ	0–0.4R_c
Impactor radius	R_{imp}	200–800 km
Impactor core radius (=diapir size)	R_{Fe}	100–400 km
Initial gap thickness	h_0	580 km
Average density of the planet	ρ_0	4060 kg m^{-3}
Iron density	ρ_{Fe}	8000 kg m^{-3}
Silicate density	ρ_{Si}	3500 kg m^{-3}
Density difference (=$\rho_{Fe} - \rho_{Si}$)	$\Delta\rho_0$	4500 kg m^{-3}
Average coefficient of thermal expansion	α	4.5×10^{-5} K^{-1}
Iron coefficient of thermal expansion	α_{Fe}	1.5×10^{-5} K^{-1}
Silicate coefficient of thermal expansion	α_{Si}	5×10^{-5} K^{-1}
Iron heat capacity	$C_{p,Fe}$	800 J K^{-1} kg^{-1}
Silicate heat capacity	$C_{p,Si}$	1000 J K^{-1} kg^{-1}
Average specific heat of the target body	$\overline{\rho_0 C_p}$	4×10^6 J K^{-1} m^{-3}
Buoyancy ratio	Γ	94
Iron latent heat	L_{Fe}	2.7×10^5 J kg^{-1}
Silicates latent heat	L_{Si}	4×10^5 J kg^{-1}
Pre-impact mantle temperature	T_0	1600 K
Pre-impact core temperature	T_c	2000 K
Heat diffusivity	χ	10^{-6} m^2 s^{-1}
Thermal conductivity	$k = k_{Si} = k_{Fe}$	4 W m^{-1} K^{-1}
Metal content	f_0	12.5%
Reference viscosity	η_0	10^{20}–10^{22} Pa s
Viscosity ratio between the hot metallic diapir and the surrounding mantle	λ_0	10^{-2}–1
Impact energy conversion coefficient	γ	0.3
Volume effectively heated by impact over the impactor volume	h_m	2.7
Surface gravity	g_0	3.85 m s^{-2}
Core surface gravity	g_c	$=g_0$
Gravitational constant	G	6.67×10^{-11} m^3 kg^{-1} s^{-2}
Average magnetic field strength	$\overline{B}$	2.5 mT
Magnetic diffusivity	ν	2 m^2 s^{-1}
Magnetic permeability	μ	$4\pi \times 10^{-7}$ H m^{-1}
Stokes regime geometrical constant	a_0	4/15–1/3
"Early time" regime geometrical constant	a_1	1/9
"Late time" regime parameter	a_2	1.3×10^{-9} m s$^{1/3}$

cur in both the mantle and the diapir (Section 4.4.3) (Samuel and Tackley, 2008; Monteux et al., 2009).

4.1. Physical model: Descent of a single diapir

To investigate the dynamics of the metallic diapir, we adapt the numerical finite volume model in spherical axisymmetric geometry of Monteux et al. (2009). We assume that the mantle is deforming in a diffusion creep limit. Conservation of energy applied to a planet of radius R then leads to

$$\frac{DT}{Dt} = \frac{\nabla^2 T}{Ra_\chi} + Di\left(\frac{\eta}{\eta_0}\Gamma\Omega - v_r\left(T + \frac{T_0}{\Delta T_0}\right)r\right), \tag{6}$$

where T, t and r are dimensionless temperature, time and radius. v_r is the dimensionless radial velocity. $Ra_\chi = \frac{\Delta\rho_0 g_0 R^3}{\chi\eta_0}$ is the compositional Rayleigh number, $Di = \frac{\alpha\rho_0 g_0 R}{\rho_0 C_p}$ is the dissipation number and $\Gamma = \Delta\rho_0/(\rho_0\alpha\Delta T_0)$ is the buoyancy ratio (Table 1). Within the target planetary mantle gravity is set equal to a constant: $g_0 = \frac{4}{3}G\pi\rho_0 R$. Within the planetary core, however, gravity is proportional to r, where $g(r) = g_0\frac{r}{R_c}$. Last, Ω is the dimensionless dissipation function and expresses the conversion of potential energy into heat through viscous dissipation:

$$\Omega = 2\underline{\varepsilon} : \underline{\varepsilon}. \tag{7}$$

where $\underline{\varepsilon}$ is the dimensionless shear strain rate tensor. Prior to impact, we assume a homogenous temperature, T_0, in the martian mantle. The viscosity is $\eta = \eta_0\lambda_0^T$, where λ_0 is the ratio (<1) of the viscosity of the hottest material (iron or silicates) to that of the colder, surrounding solid silicate mantle far from the impact site where $T = T_0$ (see value in Table 1). This viscosity decreases sharply with temperature and its expression is simpler to implement than the usual Arrhenius law (Ratcliff et al., 1997; Ziethe and Spohn, 2007). We neglect the compositional dependence of the viscosity as this effect will be much smaller than the temperature-dependence. η_0 is the reference viscosity of mantle material far from the impact site (see value in Table 1). The viscosity contrast between molten iron and mantle under martian conditions may exceed 10–20 orders of magnitude, depending on the mantle temperature. Such viscosity variations are impossible to resolve with our numerical method. However, experiments show that the dynamic influence of these large viscosity variations on diapir sinking are similar to viscosity variations of order 10^2 (Jellinek et al., 2003; Thayalan et al., 2006), the effects of which we can explore parametrically.

The other dimensionless governing equations are continuity

$$\nabla\cdot\mathbf{v} = 0, \tag{8}$$

and momentum conservation, assuming infinite Prandtl number

$$-\nabla P + \nabla\cdot\left(\frac{\eta}{\eta_0}[\nabla\mathbf{v} + [\nabla\mathbf{v}]^T]\right) + \left(\frac{T}{\Gamma} - f\right)r\mathbf{e_r} = 0, \tag{9}$$

where $\mathbf{v}$ and P are the non-dimensional velocity and pressure and $\mathbf{e_r}$ is the radial unit vector. Coupling core and mantle convection models is a difficult problem, given the different timescales and material properties for each layer. We assume here that Eq. (9) is also valid in the core. The core and the mantle are both treated as highly viscous materials. In reality, the viscosity of the core is much smaller than the mantle viscosity and the assumption that Prandtl number is

infinite is no longer valid. We will return to this issue in the conclusion.

The buoyancy force that drives the flow of the diapir towards the center of the protoplanet increases with the metallic volume fraction f that varies between 0 (pure silicates) and 1 (pure metal). The metal volume fraction f is then simply advected by the flow:

$$\frac{Df}{Dt} = 0. \tag{10}$$

4.2. Numerical model

We implement a finite volume numerical model to solve Eqs. (6), (8), (9) and (10) in axisymmetric spherical geometry. We use a stream function formulation for the equations of motion with a direct implicit inversion method (Schubert et al., 2001). Eqs. (6) and (10) are solved by an Alternating Direction Implicit (ADI) scheme (Peaceman and Rachford, 1955; Douglas, 1955). The stream function, temperature and compositional fields are described by a second-order approximation in space. To limit numerical diffusion when solving the transport equations, especially for the compositional field, we use a Total Variation Diminishing Superbee scheme (Roe, 1986; Laney, 1998) implemented in an implicit way (Srámek et al., 2010) which enables high resolution of pure advective fields. To avoid any singularity at the center of the planet, we use a staggered grid mesh (see Patankar (1980) for details) where the steam function is calculated at the corners and the temperature and compositional fields are calculated at the center of the grid cells. We use at least 200 grid points along the r-direction (i.e. the resolution $dr = 17$ km) and 400 grid points along the θ direction (i.e. the resolution $d\theta = 0.45°$). Hence the grid-point density is slightly larger towards the center of the planet. Velocity boundary conditions are free-slip at the surface and along the symmetry axis. Thermal boundary conditions are isothermal at the surface and insulating along the symmetry axis.

4.3. Analytical model of the core merging process

Buoyancy-driven interactions between two deformable viscous drops has been widely studied both experimentally and numerically (Davis et al., 1989; Yiantsios and Davis, 1990; Manga and Stone, 1993). Building on this body of work, we characterize the interaction between the preexisting core and the sinking diapir by monitoring the gap thickness, h, which is the thickness of the mantle layer between the base of the diapir and the CMB, measured along the axis of symmetry of the diapir (Fig. 2). We compare the results from our numerical models with analytical predictions. We consider the initial time t_0 to be the time at which the impact occurs.

During sinking, a diapir will deform the surrounding mantle over a radial distance that depends on the diameter of the diapir, the effective viscosities of the mantle and core, the gap thickness and the density difference across the CMB. When the diapir is small in comparison with the mantle depth and far from the core–mantle boundary, interactions with the core are negligible (Fig. 2, left). If we also neglect deformation of the density interface forming the upper boundary of the mantle the diapir sinks in the "Stokes regime" with a velocity given by Hadamard (1911) and Rybczynski (1911)

$$v = -\frac{dh}{dt} = \frac{a_0 \Delta\rho_0 g_0 R_{Fe}^2}{\lambda_0 \eta_0}, \tag{11}$$

where a_0 is a geometrical constant. In the case of a diapir sinking in an infinite medium, a_0 is given by the Hadamard–Rybczynski equation and varies from $4/15 = 0.27$ (isoviscous) to $1/3 = 0.33$ for an inviscid sphere (Hadamard, 1911; Rybczynski, 1911).

Integrating Eq. (11) with h_0 as the initial gap thickness,

$$h(t) = h_0\left(1 - \frac{t}{t_s}\frac{R_{Fe}}{h_0}\right). \tag{12}$$

Here t_s is the characteristic time for diapir descent in this regime and is given by

$$t_s = \frac{R_{Fe}}{v} = \frac{\lambda_0 \eta_0}{a_0 \Delta\rho_0 g_0 R_{Fe}} \tag{13}$$

For the impactor size range studied here, the diapir is not necessarily small in comparison to the mantle and the Stokes regime described above is not valid. As the diapir descends and $h \sim R_{Fe}$, mantle flow interacts increasingly with the CMB (Fig. 2, middle). The sinking velocity in this "Early time" regime is modified from Eq. (11) and has the form (Yiantsios and Davis (1990)):

$$v(t) = -\frac{dh}{dt} = \frac{a_1 \Delta\rho_0 g_0 R_{Fe}^{3/2} h(t)^{1/2}}{\lambda_0 \eta_0} \tag{14}$$

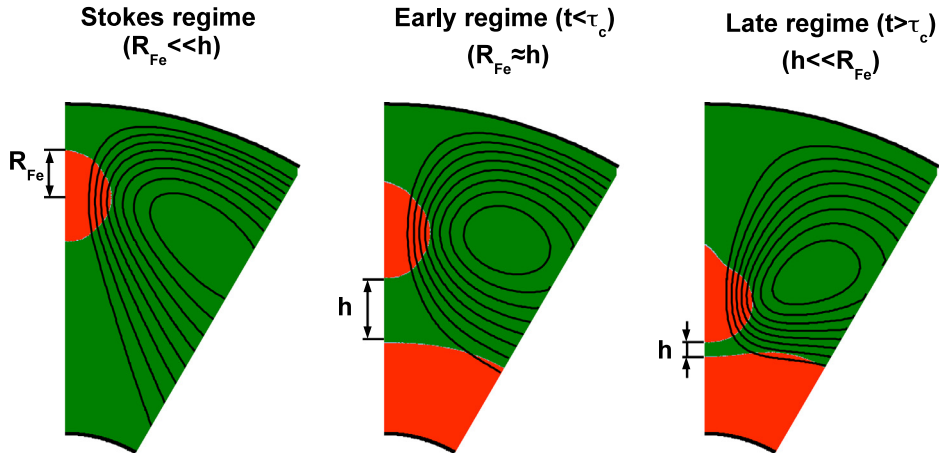

Fig. 2. Dynamics of core merging for the three regimes described in Section 4.3 and computed for $R_{Fe} = 300$ km sinking in an isoviscous differentiated Mars size planet (silicate material is represented in green and metallic material is represented in red). These results are obtained from the numerical model described in the article. Solid black lines illustrate the streamlines resulting from the diapir sinking. In the left figure, the planetary core is not present to illustrate its negligible influence on the sinking dynamics when the diapir is far from it. In this case, the viscous stress scales with $1/R_{Fe}$ (Hadamard, 1911; Rybczynski, 1911). In the middle figure, the interaction with the core results in viscous stresses that scale with $1/h$. In the right figure where $h < R_{Fe}$, interactions between the diapir and the merging core increase and the lubrication force scales with $1/h$ (Yiantsios and Davis, 1990). (For interpretation of the references to color in this figure legend, the reader is referred to the web version of this article.)

where a_1 is a geometrical constant that we determine from our numerical models. Integration of Eq. (14) with the same initial condition leads to

$$h(t) = h_0\left(1 - \frac{t}{t_c}\right)^2 \tag{15}$$

and identifies a characteristic time for diapir descent that is governed primarily by the mantle viscosity (Yiantsios and Davis, 1990):

$$t_c = \frac{2\lambda_0\eta_0}{a_1\Delta\rho_0 g_0 R_{Fe}}\left(\frac{h_0}{R_{Fe}}\right)^{1/2}. \tag{16}$$

In contrast to Eq. (13), this sinking time depends on the ratio (R_{Fe}/h_0). When $h \to 0$, $v \to 0$ (Eq. (14)) and the merging time increases towards infinity as a result of the large lateral pressure gradients required to drive viscous mantle out of the way of the sinking diapir. Indeed, Eq. (15) is strictly valid only where $t \leqslant t_c$. At "Late time" $(t/t_c \to \infty)$ the gap becomes very thin and is expected to evolve with a form (Jones and Wilson (1978) and Yiantsios and Davis (1990)):

$$h(t) = a_2 t^{-1/3} \tag{17}$$

where a_2 is a function of λ_0 and the density difference across the CMB. We obtain a_2 from our numerical results. Comparison of Eqs. (12), (15) and (17) shows that as the diapir approaches and deforms the CMB, the rate of descent will steadily decline.

4.4. Numerical results

For the range of plausible martian impactors, R_{Fe} ranges from 100 km to about 650 km. In this range, the smallest values of R_{Fe} lead to an initial Stokes regime, after which the diapir motion or gap evolution is successively described by the Early Time and Late Time regimes. Intermediate and large values of R_{Fe} lead to an initial state described by the Early Time regime, after which the motion of the diapir is described by Late Time regime. As the diapir size increases, the relative amount of time spent in the Late Time regime increases. Because the motion of the diapir in the Stoke's regime is very fast, we consider an initial gap thickness h_0 that is independent of the size of the impactor, and we model only the Early Time and Late Time regimes. We set $h_0 = 580$ km, which allows us to consider R_{Fe} in the range 100 km to a maximum value of $(R_{Mars} - R_c - h_0)/2 = 560$ km. Finally, we note that for small diapirs ($R_{Fe} < 100$ km), the Stokes regime dominates during the sinking, and conversely for very large diapirs ($R_{Fe} > 650$ km) the Late Time Regime may be the only sinking regime. Neither of these two cases is considered here.

4.4.1. Initial setup

We use the numerical model to characterize the dynamics of core merging after a giant impact on a Mars size body. First, we consider the initial martian core temperature to be homogeneous (i.e. the thickness of the thermal boundary layer $\delta = 0$) and we use the estimated present-day temperature value $T = T_{core} = 2000$ K (Williams and Nimmo, 2004). The initial thermo-chemical conditions are shown schematically in Fig. 3 in which the hatched regions represent the metallic phase from the impactor and from Mars. The initial temperature is represented with a gray scale.

4.4.2. Evolution of the gap thickness

We first monitor the thermal evolution following an impact in the absence of core merging (i.e. we consider only the thermal re-equilibration since no core merging occurs). This unphysical case is used as a control case to separate the influence of the impact heating from the diapir merging on the thermal evolution of the planet. Fig. 4 shows the thermal evolution after a 600 km impact on a Mars size body with homogeneous viscosity ($\eta_0 = 10^{22}$ Pa s). After the impact heating, the hot anomaly advects and spreads beneath the planetary surface in a few million years. Then, the hot anomaly and the target planet's core cool by diffusion.

We now consider the impactor's core. Fig. 5 shows the thermal and chemical evolution after a 600 km impact (i.e. $R_{Fe} = 300$ km) on a differentiated Mars with homogeneous viscosity ($\eta_0 = 10^{22}$ Pa s). Following the impact, a metallic diapir from the impactor forms rapidly and sinks towards the pre-existing core, while undergoing significant viscous heating. Motion of the diapir displaces surrounding mantle and deforms the CMB (Figs. 2 and 5). Merging and thermal mixing of the hot diapir into the core occurs eventually, causing the average temperature of the core to rise (Fig. 5), leading in turn, to an enhanced CMB heat flux that causes the formation and rise of a plume (Fig. 5d). The plume rising from the CMB is not the result of the onset of thermal convection in the mantle to remove the heat from the core. It is a consequence of the diapir sinking and especially of the viscous dissipation that occurs along the sinking path and generates a localized hot channel.

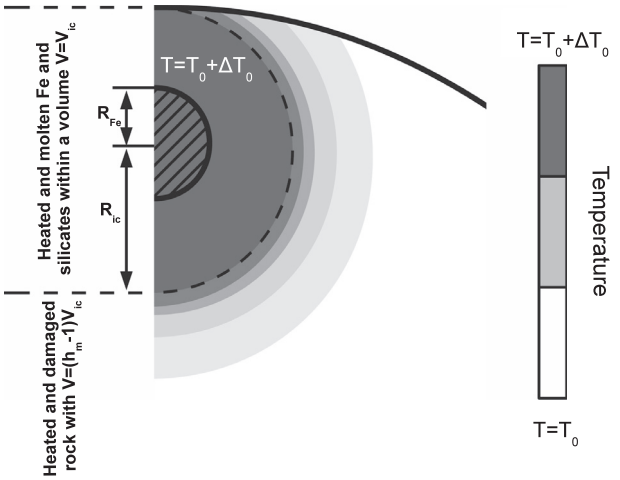

Fig. 3. Sketch to show repartitioning of the post impact heating in the martian mantle. The solid black line represents the planetary surface. Melting is restricted to the material limited by the dashed line. The impactor's core is represented by hatched lines.

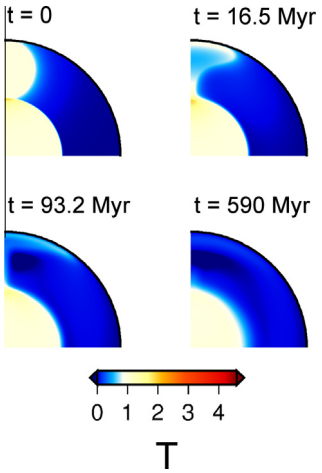

Fig. 4. Non-dimensional temperature evolution as a function of time. In this control case, we do not consider the impactor's core (computed for a uniform viscosity with $R = 3400$ km, $R_{imp} = 600$ km, $\eta_0 = 10^{22}$ Pa s and 300×600 grid points). To convert this temperature field in Kelvin, $T(K) = T_0 + T\Delta T_0$.

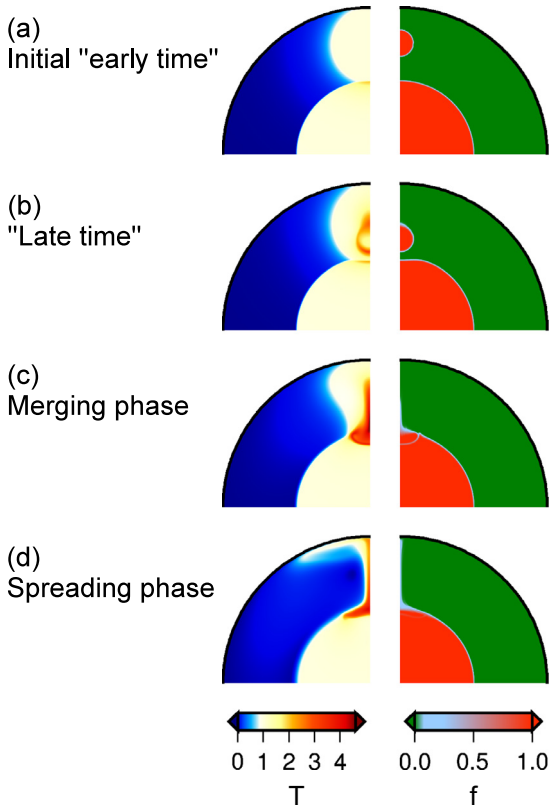

Fig. 5. Non-dimensional temperature (left) and composition (right) at times $t = 0$ (a), $t = 0.6$ Myr (b), $t = 6$ Myr (c) and $t = 38.8$ Myr (d) (computed for a uniform viscosity with $R = 3400$ km, $R_{imp} = 600$ km, $R_{Fe} = 300$ km, $\eta_0 = 10^{22}$ Pa s, $h_0 = 580$ km and 300×600 grid points). As the diapir sinks, its velocity decreases because of the increasing influence of the pre-existing core on the dynamics (see Section 4.3 for details). After the merging (c), the hot metallic fraction from the impactor spreads at the top of the martian core (d). To convert this temperature field in Kelvin, $T(K) = T_0 + T\Delta T_0$.

The plume rising does not happen in the absence of the diapir sinking (Fig. 4).

In Fig. 6, we show the temporal evolution of the gap thickness after a 600 km impact and compare it with theoretical predictions from Eqs. (15) and (17) to obtain characteristic coalescence times t_c

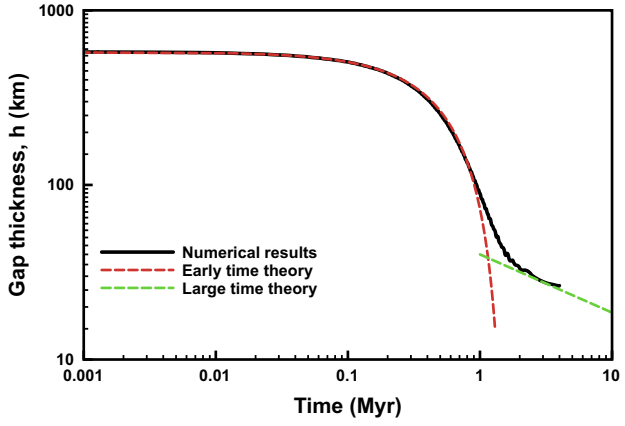

Fig. 6. Evolution of the gap thickness between the merging core and the CMB with $R_{imp} = 600$ km (i.e. $R_{Fe} = R_{imp}/2 = 300$ km). Theoretical evolutions for early times from Eq. (15) and late times from Eq. (17) are shown with red and green dashed lines respectively. From this model, we obtain a coalescence time, $t_c = 1.55$ Myr and $a_2 \sim 1.3 \times 10^9$ m s$^{1/3}$. (For interpretation of the references to color in this figure legend, the reader is referred to the web version of this article.)

and values for a_2. We repeat this for a range of plausible impactor sizes. Consistent with Eq. (16), our numerical values for t_c decrease in proportion to $R_{Fe}^{-3/2}$ (red circles, Fig. 7). In Fig. 7, we fit the numerical t_c values with the analytical prediction (black dashed line, Fig. 7) from Eq. (16) and obtain $a_1 = 1/9$.

4.4.3. Influence of the temperature-dependence of the mantle viscosity on the core merging timescale

The viscosity contrast between the sinking diapir and its environment is a key parameter in understanding the core merging dynamics. Qualitatively, as the metallic diapir sinks, shear heating occurs at the interface of the diapir (Samuel et al., 2010) and both the temperature of the diapir and the surrounding mantle can increase. Depending on the effective viscosity contrast between the metallic diapir and the mantle, the mean temperature increase within the sinking diapir can reach a maximum value $\approx 2\Delta T_0$ (Monteux et al., 2009). This temperature excess drives a heat flux from the diapir to the surrounding mantle, leading to the progressive growth of a thermal boundary layer (Fig. 5). Because the mantle viscosity declines exponentially with increasing temperature, mantle shear will be increasingly concentrated within the hottest, low viscosity part of this thermal boundary layer (Morris, 1982; Thayalan et al., 2006). Thus, heat transfer from the diapir will reduce both the effective viscosity retarding diapir motion and the radial length scale over which viscous deformation in the mantle occurs. The timescale for merging will consequently decline as a result of two processes. First, the lubricating effect of an enveloping layer of low mantle viscosity will cause metallic diapirs to descend more rapidly (cf. Eq. (14)). Second, localization of shear within only the narrow, hottest part of the thermal boundary layer will enable diapirs to more closely approach the CMB before interacting with the core.

We explore these effects quantitatively in Fig. 8, which shows analytical and numerical solutions for the evolution of the gap thickness h for a range of background mantle viscosities and diapir/mantle viscosity ratios. In the isoviscous case ($\lambda_0 = 1$), when the average viscosity decreases in the mantle (from $\eta_0 = 10^{22}$ Pa s, black solid line to $\eta = 10^{20}$ Pa s, gray solid line), the diapir sinks faster (see Eq. (14)). Consequently, the sinking time values obtained by fitting our numerical results with Eq. (15) decrease by two orders of magnitude (see Table 2).

Theoretical, experimental and numerical models (Morris, 1982; Jellinek et al., 2003; Thayalan et al., 2006) show that whereas in the isoviscous case radial mantle deformation scales with the size of the diapir, R_{Fe}, in the temperature-dependent case deformation is confined to the hottest, low viscosity part of the thermal boundary layer with a length scale typically $\sim 0.1 R_{Fe}$. As a consequence, the value of a_1 obtained by fitting our numerical results with Eq. (16) increases (see Table 2) and the sinking time value for ($\eta_0 = 10^{22}$ Pa s, $\lambda_0 = 0.01$) is smaller than for ($\eta_0 = 10^{20}$, $\lambda_0 = 1$).

5. Effect on a preexisting dynamo

We now discuss the consequences of a giant-impact and the subsequent core merging process on the martian dynamo. We first revisit the core heat flux conditions required for dynamo generation. Next, we explore the influence of core merging on the efficiency of core cooling, and thus dynamo action, for different pre-impact mantle thermal regimes.

5.1. Conditions required for dynamo generation

As discussed in Monteux et al. (2011), three conditions are required to generate a dynamo on a growing planet:

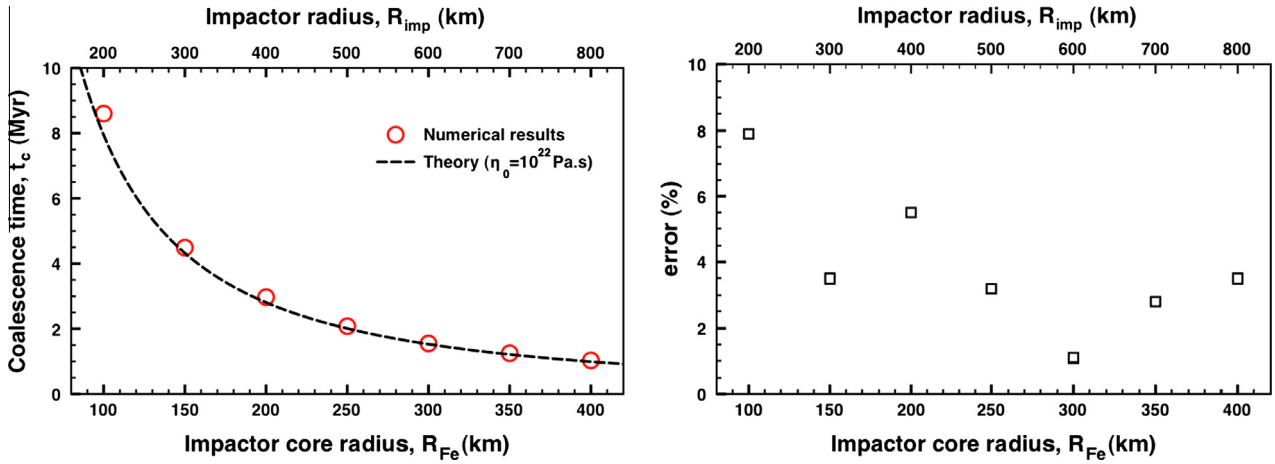

Fig. 7. Characteristic coalescence time, t_c (left panel) as a function of the impactor core radius R_{Fe}. Results from numerical experiments (with uniform viscosity $\eta_0 = 10^{22}$ Pa s and $h_0 = 580$ km) are represented with red circles. Theoretical fit from Eq. (16) is shown with the black dashed line ($a_1 = 1/9$). The corresponding errors between the numerical and theoretical models are plotted in the right panel. (For interpretation of the references to color in this figure legend, the reader is referred to the web version of this article.)

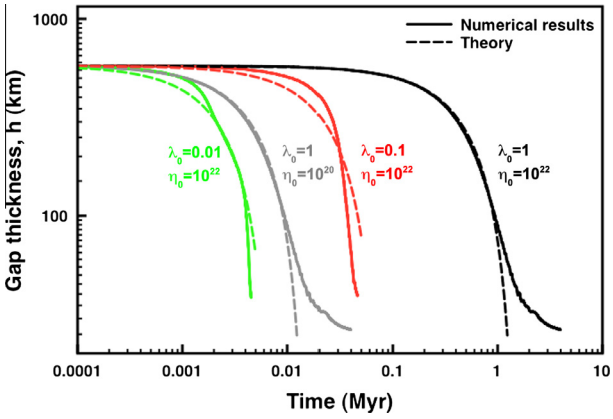

Fig. 8. Time evolution of the gap thickness between the sinking core and the pre-existing core for four different rheologies. Solid black line and solid gray line represent results from uniform viscosity models with $\eta_0 = 10^{22}$ Pa s and $\eta_0 = 10^{20}$ Pa s respectively. Solid red line and solid green line represent results from temperature dependent viscosities with $\lambda_0 = 0.1$ and $\lambda_0 = 0.01$ respectively (with $\eta = \eta_0 \lambda_0^T$ and $\eta_0 = 10^{22}$ Pa s). Theoretical predictions are shown in the corresponding color with dashed lines for the coalescence theory (Eq. (15)). (For interpretation of the references to color in this figure legend, the reader is referred to the web version of this article.)

Table 2
Sinking time values obtained fitting numerical experiments with theoretical predictions (Eq. (15)) for different values of η_0 and λ_0 (with $R_{imp} = 600$ km, $h_0 = 580$ km).

	$\eta_0 = 10^{22}$ Pa s $\lambda_0 = 1$	$\eta_0 = 10^{20}$ Pa s $\lambda_0 = 1$	$\eta_0 = 10^{22}$ Pa s $\lambda_0 = 0.1$	$\eta_0 = 10^{22}$ Pa s $\lambda_0 = 0.01$
t_c	1.56×10^3 kyr	15.6 kyr	79 kyr	7.5 kyr
a_1	0.11	0.11	0.21	0.23

1. The mean heat flux q_{CMB} out of the core must exceed the adiabatic value q_A such that convection can occur (Stevenson et al., 1983). This condition is

$$q_{CMB} > q_A = \frac{k_{Fe}\alpha_{Fe}g_c T_c}{C_{p,Fe}} \tag{18}$$

where k_{Fe}, α_{Fe}, T_c and $C_{p,Fe}$ are respectively the thermal conductivity, the coefficient of thermal expansion, the temperature and the heat capacity of the metallic phase and g_c is the gravity at the surface of the protocore. The largest uncertainties in the calculation of q_A are related to T_c and k_{Fe}. Assuming reasonable values, convection in the martian core should start once $q_{CMB} > q_A = 5 - 19$ mW m^{-2} (Nimmo and Stevenson, 2000) (see Table 1 for values).

2. The ratio of the rate at which gravitational potential energy is released by convection to the rate of ohmic dissipation, Φ, must exceed a critical value (Buffett, 2002):

$$\frac{4\pi R_c^2 q_{CMB}}{\Phi} > \frac{1}{\epsilon_T}. \tag{19}$$

where ϵ_T is the Carnot-style efficiency for thermal convection. Here, we do not consider the effect of compositional convection or the presence of an inner core. Assuming that the characteristic scale of core flow leading to magnetic field generation is the radius of the protocore, Φ can be approximated as (Buffett, 2002):

$$\Phi = \frac{4}{3}\pi R_c \left(\frac{\nu \bar{B}^2}{\mu}\right), \tag{20}$$

where $\bar{B}$ is the average strength of the magnetic field within the core, ν is the magnetic diffusivity and μ is the magnetic permeability (see Table 1 for values). In the absence of constraints on $\bar{B}$ for early planets, we assume a current Earth-like value of 2.5 mT (Kuang and Bloxham, 1997) that is independent of the protocore size or the planetary radius. The efficiency of thermal convection is given by Buffett (2002)

$$\epsilon_T = \frac{0.8\pi}{3}\frac{\alpha_{Fe} G \rho_{Fe} R_c^2}{C_{p,Fe}}\left(1 - \frac{q_A}{q_{CMB}}\right), \tag{21}$$

with ρ_{Fe} the density of the metallic phase and G the gravitational constant.
Hence Eqs. (19)–(21) along with values from Table 1 lead to:

$$q_{CMB} - q_A > \frac{\nu \bar{B}^2 C_{p,Fe}}{0.8\pi G \mu \alpha_{Fe} \rho_{Fe} R_c^3} \approx 8 \times 10^{-2} \text{ mW m}^{-2} \tag{22}$$

3. The structure of the convective motions carrying magnetic field lines must be sufficiently complicated to favor self-sustaining dynamo action. A measure of this complexity is that the magnetic Reynolds number (Christensen and Aubert, 2006) must exceed a critical value:

$$Re_m = \frac{UL}{\nu} > Re_m^{crit} = O(10 - 10^2) \tag{23}$$

Here, L and U are the characteristic length and velocity scales for the flow within the protocore and ν is the magnetic diffusivity of the metal phase. The natural length scale in the problem is the depth of the convecting iron layer, however the velocity scale depends on the leading order force balance (Christensen, 2010). As the rotation rate of growing planets is potentially time-dependent and poorly constrained, a convenient and reasonable choice is based on a balance between inertial and buoyancy forces and is (Stevenson, 2003):

$$U \sim \left(\frac{(q_{CMB}-q_A)\alpha_{Fe} g_c R_c}{\rho_{Fe} C_{p,Fe}}\right)^{1/3}, \tag{24}$$

Taking $L = R_c$ and $Re_m^{crit} = 10^2$, the combination of Eqs. (23) and (24) leads to the condition

$$q_{CMB} - q_A > \frac{\rho_{Fe} C_{p,Fe}}{\alpha_{Fe} g_c R_c}\left(Re_m^{crit}\frac{\nu}{R_c}\right)^3 \approx 10^{-4}\ \mathrm{mW\ m^{-2}} \tag{25}$$

Among the three criteria above, the first is typically considered a necessary condition for a thermally-driven dynamo (subadiabatic dynamos are possible if compositional buoyancy effects enter the problem). It is not a sufficient condition for dynamo action, as indicated by the other two conditions. However, conditions 2 and 3 require that the heat flux q_{CMB} at the CMB be only about 1% greater than the adiabatic heat flux q_A. Thus, we take q_A to be a reasonable critical value for dynamo generation (Stevenson et al., 1983; Nimmo and Stevenson, 2000; Williams and Nimmo, 2004).

5.2. Thermal consequences of the core merging

5.2.1. CMB cooling

To understand the influence of the merging process on thermally-driven dynamo action, we first specify the thermal structure and cooling regime of the core prior to merging, which depends on the previous accretion and core formation histories (Monteux et al., 2009; Samuel et al., 2010). Two end-member models for the initial interior thermal state of Mars are the isothermal case with the core and the mantle having the same temperature, and a situation where the core is much hotter than the mantle. In the case of a pre-impact core hotter than the mantle, the thickness δ of the thermal boundary layer (TBL), across which temperature declines linearly from the core to the mantle value is governed by the mode of heat loss to the mantle. Strong cooling to the mantle leads to thin thermal boundary layers and vigorous convection, weak cooling leads to relatively more sluggish flow or no convection at all. To simplify this problem we consider three pre-impact core thermal states: an isothermal core and mantle (uniform temperature), and two models where the core is hotter than the mantle with $\delta = 0.1R_c$ (strong core cooling) and $\delta = 0.4R_c$ (weak core cooling and no core convection).

Our results show that one major consequence of large impacts is to heat the mantle and reduce the temperature difference between the core and mantle (where there is one initially) and, thus the CMB heat flux (Roberts et al., 2009). Where a metallic diapir forms and descends such that it becomes hotter than the pre-existing core, merging can lead to the spread of a thin, hot, gravity current along the CMB. If the timescale for spreading t_{spread} is much smaller than the timescale for thermal diffusion t_{diff} across the current then this stratification can insulate the core against the mantle. This can in turn drive a heat flux into the core itself and inhibit dynamo action (Arkani-Hamed and Olson, 2010).

In the uniform temperature case, following merging and coalescence (Fig. 9, top-left panel, solid circles) an increase in the CMB heat flux occurs at $\sim 10t_c$ because the production of thermal stratification increases the temperature difference to the mantle. The magnitude of this temperature difference increases with rate of spreading relative to the rate at which thermal diffusion smoothes temperature variations. Thus, the largest diapirs spreading in the lowest viscosity cores are characterized by the greatest increases in CMB heat flux (green curve). By contrast, in the weak and strong core cooling cases, initial mantle heating causes a reduction in the CMB heat flux following coalescence that is followed, in turn, by an increase in this heat flux until $t/t_{diff} \rightarrow 1$. The magnitude of this increase is in proportion to the strength of the resulting thermal stratification. As in the uniform temperature case, the greatest CMB heat fluxes then correspond with the largest diapirs and lowest viscosity cores (green curves). Notably, the smallest and most slowly spreading diapir in the strong cooling regime (Fig. 9, red curve) produces no significant stratification because $t_{spread}/\ t_{diff} \gg 1$.

5.2.2. Merging, stratification and thermal mixing: Potential effect on an early Mars dynamo

Material from our lowest viscosity and largest diapirs spreads along the CMB as a thin, axisymmetric gravity current. In the limit that this spreading is under the zero Reynolds number conditions of our numerical simulations, the radius of the current will increase at a rate that is approximately proportional to time $t^{1/8}$ (Huppert, 1982) to form a hot, stratified layer that insulates the core and inhibits core convection and dynamo action (Fig. 9, green curves) (Arkani-Hamed and Olson, 2010). This thermal stratification persists until the thermal anomaly introduced by the gravity current has diffused into the overlying mantle and underlying core. Where weak or no stratification is produced, merging and spreading weakens core convection as a result of mantle heating but will not necessarily destroy a pre-existing dynamo (Fig. 9, blue and red curves).

In reality, the gravity current driven as a result of the merging of a $\sim$400 km radius diapir carrying $\sim$800 K temperature variations can spread in a very low viscosity core under finite-or even high-Re conditions. In the high-Re limit, at large times where the current is thin in comparison to its radius, the radius of the current will increase in proportion to $t^{1/2}$ (Kotsovinos, 2000) and may involve extensive mixing across the density interface forming the base of the flow, depending on the magnitude of the temperature difference, the thickness of the flow and the rotation rate of Mars (Linden, 1977; Linden, 1979; Fleury et al., 1991; Kotsovinos, 2000).

A careful consideration of the efficiency of thermal mixing across this density interface requires a different numerical model and is beyond the scope of this paper. However, it is useful to explore the end-member case of perfect thermal mixing in order to determine the maximum core heat flux that is likely to occur after merging, spreading and thorough mixing. To obtain a crude estimate of the effects of complete thermal mixing of the hot gravity current into the underlying core, we stir in the gravity current at $t = t_{spread}$ and then determine the mean temperature of the core $\overline{T_c}$ and the corresponding CMB heat flux (Fig. 10, solid square). Because spreading and mixing in a high-Re limit will occur on a timescale that is much smaller than t_{diff} (i.e., for $t_{spread} \ll t_{diff}$), we explore only the effect of stirring in the stratified layer corresponding to the largest, lowest viscosity diapir in Fig. 9 (Fig. 10). In Fig. 10, the discontinuity in the heat flux evolution is the consequence of imposing a new thermal state. The main effect of an imposed mixing event at $t = t_{spread}$ is to reduce the average core temperature to a value intermediate between the initial and fully stratified cases (Fig. 10). Whereas the peak in the CMB heat flux corresponds to stratification that would likely destroy the dynamo (cf., Fig. 9), the lower, post-mixing, heat flux can drive a dynamo for several diffusion times, which corresponds to a few hundred million years.

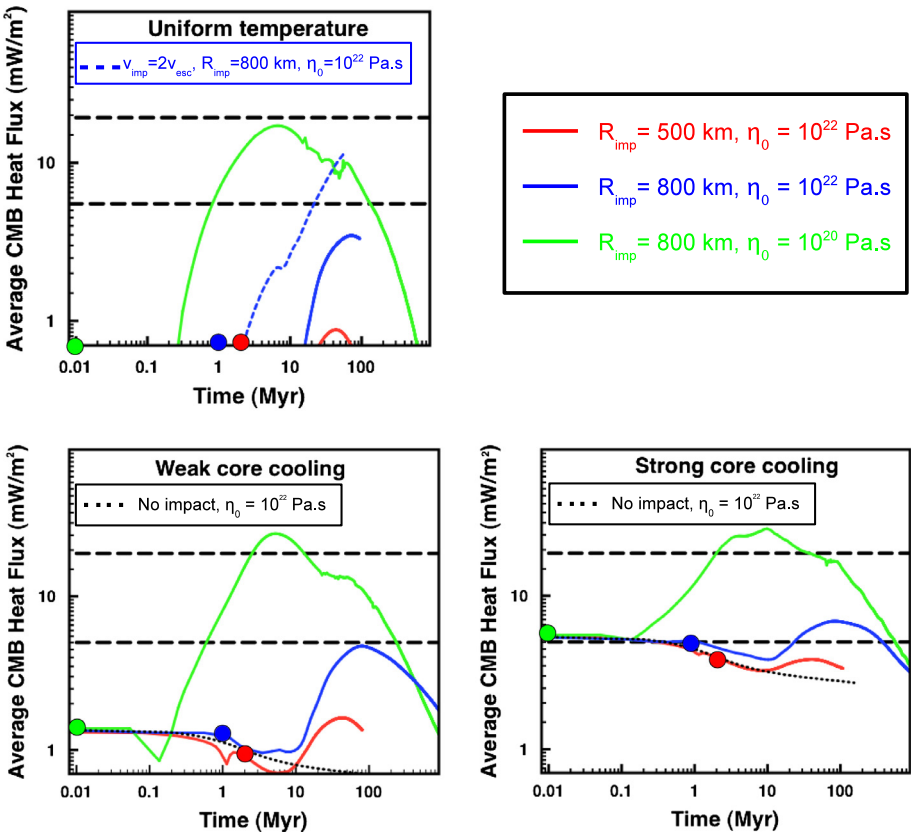

Fig. 9. Time evolution of the mean CMB heat flux in the stratified case as a function of the viscosity and impactor size. The characteristic diffusion time $t_{diff} = d^2/\kappa$, where the steady-state thickness d is defined where the spreading gravity current extends over 25% of the CMB. In the three panels different initial thermal states before impact are considered. The two horizontal black dashed lines represent the theoretical dynamo criterion for q_{CMB} ($q_{CMB} > q_A = 5 - 19$ mW m^{-2}). In the top-left panel, pre-impact temperature is assumed to be constant ($T = T_0$). In the bottom panels, the core is initially hotter than the mantle $T = T_{core} > T_0$. The black dotted lines represent q_{CMB} in the absence of an impact. In the bottom left panel the CMB thermal boundary layer thickness $\delta = 0.4R_{Fe}$ and in the bottom right panel $\delta = 0.1R_{Fe}$. Red, blue and green solid lines represent the evolution with ($R_{imp} = 500$ km, $\eta_0 = 10^{22}$ Pa s), ($R_{imp} = 800$ km, $\eta_0 = 10^{22}$ Pa s), and ($R_{imp} = 800$ km, $\eta_0 = 10^{20}$ Pa s) respectively. In the top-left panel, the blue dashed line is the result of the same model as the solid blue line but with $v_{imp} = 2v_{esc}$ (i.e. the post-impact temperature increase is ≈4 times larger). Filled circles represent the coalescence times t_c/t_{diff} from Eq. (16). In the weak and strong core cooling cases, the mean heat flux decreases for $t_c/t_{diff} < t/t_{diff} < 10t_c/t_{diff}$ because of the post-impact mantle thermal anomaly that inhibits the CMB heat loss. The combination of the spreading and cooling mantle thermal anomaly, and of the thermal core stratification leads to an increase of the CMB heat flux after $t \sim 10t_c/t_{diff}$. The maximum average heat flux increase at the CMB is reached when $R_{imp} = 800$ km and when $\eta_0 = 10^{20}$ Pa s. (For interpretation of the references to color in this figure legend, the reader is referred to the web version of this article.)

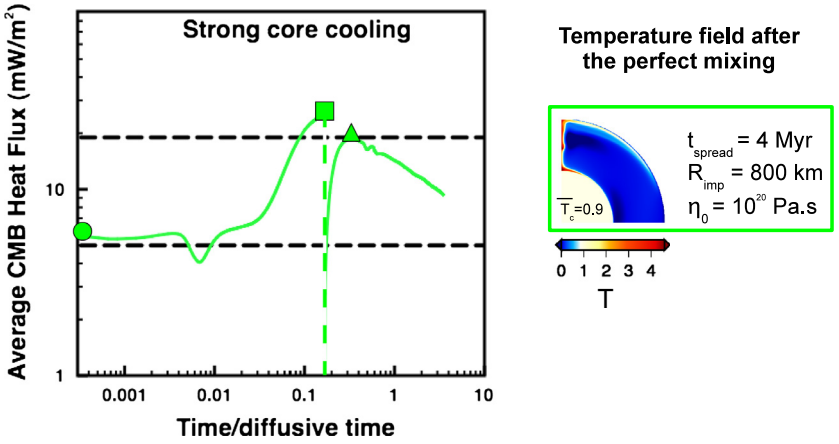

Fig. 10. Time evolution of the mean CMB heat flux in the perfect mixing case as a function of the viscosity and impactor size. The characteristic diffusion time $t_{diff} = d^2/\kappa$, where the steady-state thickness d is defined where the spreading gravity current extends over 25% of the CMB. Here $t_{diff} = 27.8$ Myr. Perfect thermal mixing is imposed within the core when $t = t_{spread}$ (vertical dashed line). The two horizontal black dashed lines represent the theoretical dynamo criterion for q_{CMB} ($q_{CMB} > q_A = 5 - 19$ mW m^{-2}). The green solid line represent the evolution with ($R_{imp} = 800$ km, $\eta_0 = 10^{20}$ Pa s, $t_{spread} = 4$ Myr). The filled circle represents the coalescence times (t_c/t_{diff}) from Eq. (16), the filled square represents the spreading time (t_{spread}/t_{diff}) and the filled triangle represents the relevant mean heat flux after thermal mixing. The right panel shows the corresponding non-dimensional temperature field right after the perfect mixing. To convert this temperature field in Kelvin, $T(K) = T_0 + T\Delta T_0$. (For interpretation of the references to color in this figure legend, the reader is referred to the web version of this article.)

6. Conclusions

Giant impacts may have played an important role in the thermal and magnetic evolutions of terrestrial planets. The giant impact potentially forming the martian dichotomy could have supplied a significant volume of iron that merged with the preexisting core. We model the dynamics of the sinking of a large metallic diapir within a silicate mantle and the influence of the deformation of the preexisting core on the merging process. We obtain characteristic timescales of the coalescence time between the two cores as a function of the viscosity of the mantle and the size of the sinking diapir. Our results are in agreement with theoretical and experimental models of buoyancy-driven motions sinking toward a deformable surface. We also show that the thermal consequences of the merging process can influence the generation of a martian dynamo. Assuming perfect thermal mixing, the dynamo generation might be favored by large impacts, low viscosity of the preexisting core and strong preexisting core cooling. The dynamo can last as long as several hundred million years depending on the mixing process within the core.

The novelty of our models is that we characterize and understand theoretically the sinking of a large volume of iron through a silicate mantle as well as the interactions between the two cores during the merging. Our thermal models also include the dissipation of energy via viscous heating which allows us to characterize the thermal consequences of the impactor's core sinking within the mantle and the pre-existing core. The results illustrate that the core merging is a process with a characteristic time that is essentially governed by the mechanical properties of the mantle. The dynamics and thermal consequences of the core merging process are important aspects of the giant impacts that potentially delivered large volumes of iron during the late accretionary history of terrestrial planets.

The heating induced by the impact within the mantle and the viscous dissipation during diapir sinking enhances a thermal anomaly within the mantle. These processes strongly affect the heat budget of the mantle and may have long term consequences on a planet's thermal evolution. The impact heating within the mantle leads to a dichotomy of the core cooling: the core heat flux at the CMB below the impact site is different than the CMB heat flux on the opposite side of the core. This mantle heterogeneity might affect the dynamo and the resulting paleomagnetic field recorded at the surface (Stanley et al., 2008; Sreenivasan and Jellinek, 2012). Moreover, recent dynamo simulations show that the efficiency of a mantle heterogeneity centered at the geographical pole in producing a south-north dichotomy is much higher than that of an heterogeneity centered at the equator in producing an east–west dichotomy (Amit et al., 2011). Hence, our models may have interesting implications for the understanding of the structure of the past martian dynamo.

We illustrate the importance of better constraining the thermal states of the cores, the size of the largest metallic diapir that remains after a giant impact, and the depth at which the impactor's core is buried before experiencing viscous deformation and the core merging process. We assume that the impact occurs with the martian escape velocity which is the minimum impact velocity; larger impact velocities can substantially increase the post-impact temperature in the mantle and in the merging core prior to its sinking. Hence, in this respect our results provide a lower bound on the temperature increase in the planetary core after the diapir merging and on the CMB heat flux increase (see Fig. 9, top left panel).

In our models, we make the strong assumption that the sinking impactor's core, the target silicate mantle and the target iron core are in the infinite Prandtl number regime. In reality, both the molten metallic cores have viscosities that are 10–20 orders of magnitude smaller than the mantle viscosity. Accounting for such large realistic viscosity contrasts may have consequences on both the sinking and the merging dynamics. Indeed, considering a more realistic viscosity contrast between the sinking metallic diapir and the silicate mantle may affect the heat dissipation during the sinking. Viscous heating will preferentially occur in the surrounding mantle reducing the maximal temperature reached within the merging diapir and the energy brought to the preexisting core (Monteux et al., 2009, 2011; Samuel et al., 2010). However, considering an inviscid sinking metallic diapir should not change significantly the diapir sinking velocity which is mainly governed by the mantle viscosity (Hadamard, 1911; Rybczynski, 1911; Yiantsios and Davis, 1990). Inertial and Coriolis forces can even favor dynamo generation during the sinking of the molten metallic diapir (Monteux et al., 2012). Concerning the merging dynamics, the injection of a large volume of molten iron in a turbulent and rotating preexisting core is a process that is difficult to handle numerically. To the first order, the merging dynamics is probably bounded between two extreme cases. In the infinite Prandtl number approximation, the stratification at the end of the merging is unavoidable and the core merging process will stop the preexisting dynamo. However, turbulence and rotational forces may enhance efficient thermal mixing within the preexisting core which may reactivate a dynamo previously killed by the impact heating.

Future missions will provide important additional constraints on interior structure and remanent crustal magnetic field of Mars that will help constrain interior thermal evolution and dynamo models. The MAVEN mission will provide low-altitude vector magnetic field observations at locations other than those sampled at low altitudes by Mars Global Surveyor. The InSight mission will provide constraints on the outer core radius, mantle seismic velocity structure (and hence on temperature and composition), and heat flow at a single lander location. The inference (from seismology) of any thermal dichotomy between the northern hemisphere and the southern hemisphere could be the consequence of a large core merging event. Another key to testing such models may consist of measurements of the degree of equilibration between the mantle and the core material of Mars. During the core merging following a giant impact, the metal may sink as unequilibrated blobs (Dahl and Stevenson, 2010; Kleine and Rudge, 2011). Hence, some memory of the core merging process might have been recorded in the martian mantle. An inferred dichotomy in the chemical composition of the martian mantle between the northern lowlands and the southern highlands could also be the consequence of a giant impact and of the subsequent core merging process.

Acknowledgments

J. Monteux is funded by Agence Nationale de la Recherche (Accretis decision No. ANR-10-PDOC-001-01). M. Jellinek and C.L. Johnson acknowledge support from the Natural Science and Engineering Research Council of Canada. We thank J. Roberts and anonymous reviewer for thoughtful and constructive comments.

References

Acuña, M. et al., 1999. Global distribution of crustal magnetization discovered by the Mars Global Surveyor MAG/ER experiment. Science 284, 790–793.

Agee, C.B., 1997. Melting temperatures of the Allende meteorite: Implications for a Hadean magma ocean. Phys. Earth Planet. Inter. 100, 41–47.

Amit, H., Christensen, U.R., Langlais, B., 2011. The influence of degree-1 mantle heterogeneity on the past dynamo of Mars. Phys. Earth Planet. Inter. 189, 63–79. http://dx.doi.org/10.1016/j.pepi.2011.07.008.

Andrews-Hanna, J.C., Zuber, M.T., Banerdt, W.B., 2008. The Borealis basin and the origin of the martian crustal dichotomy. Nature 453, 1212–1215. http://dx.doi.org/10.1038/nature07011.

Arkani-Hamed, J., Olson, P., 2010. Giant impact stratification of the martian core. Geophys. Res. Lett. 370 (L02), 201. http://dx.doi.org/10.1029/2009GL041417.

Asphaug, E., 2010. Similar-sized collisions and the diversity of planets. Chem. Erde/Geochem. 70, 199–219. http://dx.doi.org/10.1016/j.chemer.2010.01.004.

Benz, W., Slattery, W.L., Cameron, A.G.W., 1988. Collisional stripping of Mercury's mantle. Icarus 74, 516–528. http://dx.doi.org/10.1016/0019-1035(88)90118-2.

Buffett, B.A., 2002. Estimates of heat flow in the deep mantle based on the power requirements for the geodynamo. Geophys. Res. Lett. 29 (12), 1–4.

Canup, R.M., 2004. Simulations of a late lunar-forming impact. Icarus 168, 433–456. http://dx.doi.org/10.1016/j.icarus.2003.09.028.

Christensen, U.R., 2010. Dynamo scaling laws and applications to the planets. Space Sci. Rev. 152, 565–590.

Christensen, U.R., Aubert, J., 2006. Scaling properties of convection-driven dynamos in rotating spherical shells and application to planetary magnetic fields. Geophys. J. Int. 166, 97–114.

Citron, R.I., Zhong, S., 2012. Constraints on the formation of the martian crustal dichotomy from remnant crustal magnetism. Phys. Earth Planet. Inter. 212, 55–63. http://dx.doi.org/10.1016/j.pepi.2012.09.008.

Croft, S.K., 1982. A first-order estimate of shock heating and vaporization in oceanic impacts. In: Silver, T.L., Schultz, P.H. (Eds.), Geological Implications of Impacts of Large Asteroids and Comets on Earth, vol. 190. Spec. Pap. Geol. Soc. Am., pp. 143–152.

Ćuk, M., Stewart, S.T., 2012. Making the Moon from a fast-spinning Earth: A giant impact followed by resonant despinning. Science 338, 1047–1052. http://dx.doi.org/10.1126/science.1225542.

Dahl, T.W., Stevenson, D.J., 2010. Turbulent mixing of metal and silicate during planet accretion and interpretation of the Hf-W chronometer. Earth Planet. Sci. Lett. 295, 177–186. http://dx.doi.org/10.1016/j.epsl.2010.03.038.

Davies, G.F., 1982. Ultimate strength of solids and formation of planetary cores. Geophys. Res. Lett. 9, 1267–1270.

Davis, R.H., Schonberg, J.A., Rallison, J.M., 1989. The lubrication force between two viscous drops. Phys. Fluids 1, 77–81. http://dx.doi.org/10.1063/1.857525.

Douglas, J., 1955. On the numerical integration of $\frac{\partial^2 u}{\partial x^2}+\frac{\partial^2 u}{\partial y^2}=\frac{\partial u}{\partial t}$ by implicit methods. J. Soc. Ind. Appl. Math. 3, 42–65. http://dx.doi.org/10.1137/0103004.

Elkins-Tanton, L.T., Parmentier, E.M., Hess, P.C., 2003. Magma ocean fractional crystallization and cumulate overturn in terrestrial planets: Implications for Mars. Meteorit. Planet. Sci. 38, 1753–1771.

Ernst, C.M. et al., 2010. Exposure of spectrally distinct material by impact craters on Mercury: Implications for global stratigraphy. Icarus 209, 210–223. http://dx.doi.org/10.1016/j.icarus.2010.05.022.

Fleury, M., Mory, M., Hopfinger, E.J., Auchere, D., 1991. Effects of rotation on turbulent mixing across a density interface. J. Fluid Mech. 223, 165–191. http://dx.doi.org/10.1017/S0022112091001386.

Frey, H.V., 2006. Impact constraints on the age and origin of the lowlands of Mars. Geophys. Res. Lett. 33, L08S02. http://dx.doi.org/10.1029/2005GL024484.

Gerya, T.V., Yuen, D.A., 2007. Robust characteristics method for modelling multiphase visco-elastic thermo-mechanical problems. Phys. Earth Planet. Inter. 163, 83–105.

Hadamard, J., 1911. Mouvement permanent lent d'une sphère liquide et visqueuse dans un liquide visqueux. C.R. Acad. Sci. 152, 1735–1738.

Hartmann, W.K., Davis, D.R., 1975. Satellite-sized planetesimals and lunar origin. Icarus 24, 504–514.

Höink, T., Schmalzl, J., Hansen, U., 2005. Formation of compositional structures by sedimentation in vigorous convection. Phys. Earth Planet. Inter. 153, 11–20.

Hood, L.L., Richmond, N.C., Pierazzo, E., Rochette, P., 2003. Distribution of crustal magnetic fields on Mars: Shock effects of basin-forming impacts. Geophys. Res. Lett. 30 (6), 1–4.

Huppert, H.E., 1982. The propagation of two-dimensional and axisymmetric viscous gravity currents over a rigid horizontal surface. J. Fluid Mech. 121, 43–58.

Jellinek, A.M., Gonnermann, H.M., Richards, M.A., 2003. Plume capture by divergent plate motions: Implications for the distribution of hotspots, geochemistry of mid-ocean ridge basalts, and estimates of the heat flux at the core–mantle boundary. Earth Planet. Sci. Lett. 205, 361–378. http://dx.doi.org/10.1016/S0012-821X(02)01070-1.

Johnson, C.L., Phillips, R.J., 2005. Evolution of the Tharsis region of Mars: Insights from magnetic field observations. Earth Planet. Sci. Lett. 230, 241–254.

Jones, A.F., Wilson, S.D.R., 1978. The film drainage problem in droplet coalescence. J. Fluid Mech. 87, 263–288. http://dx.doi.org/10.1017/S0022112078001585.

Kaula, W.M., 1979. Thermal evolution of Earth and Moon growing by planetesimal impacts. J. Geophys. Res. 84, 999–1008.

Ke, Y., Solomatov, V.S., 2009. Coupled core–mantle thermal evolution of early Mars. J. Geophys. Res. (Planets) 114 (13), 1–12.

Kleine, T., Rudge, J.F., 2011. Chronometry of meteorites and the formation of the Earth and Moon. Elements 7, 41–46. http://dx.doi.org/10.1016/j.gca.2006.06.004.

Kotsovinos, N.E., 2000. Axisymmetric submerged intrusion in stratified fluid. J. Hydraul. Eng. 126, 446–456. http://dx.doi.org/10.1061/(ASCE)0733-9429(2000)126:6(446).

Kuang, W., Bloxham, J., 1997. An Earth-like numerical dynamo model. Nature 389, 371–374.

Laney, C.B., 1998. Computational Gasdynamics. Cambridge University Press, Cambridge.

Lee, D.C., Halliday, A.N., 1997. Core formation on Mars and differentiated asteroids. Nature 388, 854–857.

Lillis, R.J., Frey, H.V., Manga, M., 2008a. Rapid decrease in martian crustal magnetization in the Noachian era: Implications for the dynamo and climate of early Mars. Geophys. Res. Lett. 35 (L14), 203.

Lillis, R.J., Frey, H.V., Manga, M., Mitchell, D.L., Lin, R.P., Acuña, M.H., Bougher, S.W., 2008b. An improved crustal magnetic field map of Mars from electron reflectometry: Highland volcano magmatic history and the end of the martian dynamo. Icarus 194, 575–596.

Linden, P.F., 1977. The flow of a stratified fluid in a rotating annulus. J. Fluid Mech. 79, 435–447. http://dx.doi.org/10.1017/S0022112077000251.

Linden, P.F., 1979. Mixing in stratified fluids. Geophys. Astrophys. Fluid Dyn. 13, 3–23. http://dx.doi.org/10.1080/03091927908243758.

Manga, M., Stone, H.A., 1993. Buoyancy-driven interactions between two deformable viscous drops. J. Fluid Mech. 256, 647–683. http://dx.doi.org/10.1017/S0022112093002915.

Marinova, M.M., Aharonson, O., Asphaug, E., 2008. Mega-impact formation of the Mars hemispheric dichotomy. Nature 453, 1216–1219. http://dx.doi.org/10.1038/nature07070.

Marinova, M.M., Aharonson, O., Asphaug, E., 2011. Geophysical consequences of planetary-scale impacts into a Mars-like planet. Icarus 211, 960–985. http://dx.doi.org/10.1016/j.icarus.2010.10.032.

Monteux, J., Coltice, N., Dubuffet, F., Ricard, Y., 2007. Thermo-mechanical adjustment after impacts during planetary growth. Geophys. Res. Lett. 34, 24201–24205.

Monteux, J., Ricard, Y., Coltice, N., Dubuffet, F., Ulvrova, M., 2009. A model of metal-silicate separation on growing planets. Earth Planet. Sci. Lett. 287, 353–362.

Monteux, J., Jellinek, A.M., Johnson, C.L., 2011. Why might planets and moons have early dynamos? Earth Planet. Sci. Lett. 310, 349–359. http://dx.doi.org/10.1016/j.epsl.2011.08.014.

Monteux, J., Schaeffer, N., Amit, H., Cardin, P., 2012. Can a sinking metallic diapir generate a dynamo? J. Geophys. Res. (Planets) 117 (16), E10005. http://dx.doi.org/10.1029/2012JE004075.

Morris, S., 1982. The effects of a strongly temperature-dependent viscosity on slow flow past a hot sphere. J. Fluid Mech. 124, 1–26. http://dx.doi.org/10.1017/S0022112082002389.

Nimmo, F., Kleine, T., 2007. How rapidly did Mars accrete? Uncertainties in the Hf W timing of core formation. Icarus 191, 497–504. http://dx.doi.org/10.1016/j.icarus.2007.05.002.

Nimmo, F., Stevenson, D.J., 2000. Influence of early plate tectonics on the thermal evolution and magnetic field of Mars. J. Geophys. Res. 105, 11969–11980.

Nimmo, F., Hart, S.D., Korycansky, D.G., Agnor, C.B., 2008. Implications of an impact origin for the martian hemispheric dichotomy. Nature 453, 1220–1223. http://dx.doi.org/10.1038/nature07025.

O'Keefe, J.D., Ahrens, T.J., 1977. Impact-induced energy partitioning, melting, and vaporization on terrestrial planets. In: Merril, R.B. (Ed.), Lun. Planet. Sci. Conf., vol. 8, pp. 3357–3374.

Patankar, S.V., 1980. Numerical Heat Transfer and Fluid Flow. Series in Computational Methods in Mechanics and Thermal Sciences. Hemisphere Publishing Corp., Washington, DC, 210p..

Peaceman, D.W., Rachford, H.H., 1955. The numerical solution of parabolic and elliptic differential equations. J. Soc. Ind. Appl. Math. 3, 28–41. http://dx.doi.org/10.1137/0103003.

Pierazzo, E., Vickery, A.M., Melosh, H.J., 1997. A reevaluation of impact melt production. Icarus 127, 408–423.

Ratcliff, J.T., Tackley, P.J., Schubert, G., Zebib, A., 1997. Transitions in thermal convection with strongly variable viscosity. Phys. Earth Planet. Inter. 102, 201–212.

Reese, C.C., Solomatov, V.S., 2010. Early martian dynamo generation due to giant impacts. Icarus 207, 82–97. http://dx.doi.org/10.1016/j.icarus.2009.10.016.

Ricard, Y., Šrámek, O., Dubuffet, F., 2009. A multi-phase model of runaway core–mantle segregation in planetary embryos. Earth Planet. Sci. Lett. 284, 144–150.

Roberts, J.H., Arkani-Hamed, J., 2012. Impact-induced mantle dynamics on Mars. Icarus 218, 278–289. http://dx.doi.org/10.1016/j.icarus.2011.11.038.

Roberts, J.H., Barnouin, O.S., 2012. The effect of the Caloris impact on the mantle dynamics and volcanism of Mercury. J. Geophys. Res. (Planets) 117, E02007. http://dx.doi.org/10.1029/2011JE003876.

Roberts, J.H., Zhong, S., 2006. Degree-1 convection in the martian mantle and the origin of the hemispheric dichotomy. J. Geophys. Res. (Planets) 111 (10), E06013. http://dx.doi.org/10.1029/2005JE002668.

Roberts, J.H., Lillis, R.J., Manga, M., 2009. Giant impacts on early Mars and the cessation of the martian dynamo. J. Geophys. Res. (Planets) 114 (13), E04009. http://dx.doi.org/10.1029/2008JE003287.

Roe, P.L., 1986. Characteristic-based schemes for the Euler equations. Ann. Rev. Fluid Mech. 18, 337–365.

Rosenblatt, P., 2011. The origin of the martian moons revisited. Astron. Astrophys. Rev. 19, 44. http://dx.doi.org/10.1007/s00159-011-0044-6.

Rubie, D.C., Melosh, H.J., Reid, J.E., Liebske, C., Righter, K., 2003. Mechanisms of metal–silicate equilibration in the terrestrial magma ocean. Earth Planet. Sci. Lett. 205, 239–255.

Rybczynski, W., 1911. über die fortschreitende bewegung einer flüssigen kugel in einen medium. Bull. Acad. Sci. Cracovie 1, 40–46.

Safronov, V.S., 1978. The heating of the Earth during its formation. Icarus 33, 3–12. http://dx.doi.org/10.1016/0019-1035(78)90019-2.

Samuel, H., Tackley, P.J., 2008. Dynamics of core formation and equilibration by negative diapirism. Geochem. Geophys. Geosyst. 9, 6011–6026.

Samuel, H., Tackley, P.J., Evonuk, M., 2010. Heat partitioning in terrestrial planets during core formation by negative diapirism. Earth Planet. Sci. Lett. 290, 13–19.

Schubert, G., Turcotte, D.L., Olson, P., 2001. Mantle Convection in the Earth and Planets. Cambridge University Press.

Senshu, H., Kuramoto, K., Matsui, T., 2002. Thermal evolution of a growing Mars. J. Geophys. Res. 107, 1–13.
Shannon, M.C., Agee, C.B., 1996. High pressure constraints on percolative core formation. Geophys. Res. Lett. 23, 2717–2720.
Sleep, N.H., 1994. Martian plate tectonics. J. Geophys. Res. 99, 5639. http://dx.doi.org/10.1029/94JE00216.
Smith, J.V., 1979. Mineralogy of the planets: A Voyage in space and time. Mineral. Mag. 43, 1–89.
Srámek, O., Ricard, Y., Dubuffet, F., 2010. A multiphase model of core formation. Geophys. J. Int. 181, 198–220. http://dx.doi.org/10.1111/j.1365-246X.2010.04528.x.
Sreenivasan, B., Jellinek, A., 2012. Did the Tharsis plume terminate the martian dynamo? Earth Planet. Sci. Lett. 349, 209–217. http://dx.doi.org/10.1016/j.epsl.2012.07.013.
Stanley, S., Elkins-Tanton, L., Zuber, M.T., Parmentier, E.M., 2008. Mars' paleomagnetic field as the result of a single-hemisphere dynamo. Science 321, 1822–1825. http://dx.doi.org/10.1126/science.1161119.
Stevenson, D.J., 1989. Formation and early evolution of the Earth. In: Peltier, W.R. (Ed.), Mantle Convection and Plate Tectonics, pp. 818–868.
Stevenson, D.J., 2001. Mars' core and magnetism. Nature 412, 214–219.
Stevenson, D.J., 2003. Planetary magnetic fields. Earth Planet. Sci. Lett. 208, 1–2.
Stevenson, D.J., Spohn, T., Schubert, G., 1983. Magnetism and thermal evolution of the terrestrial planets. Icarus 54, 466–489.
Thayalan, V., Jellinek, A.M., Lenardic, A., 2006. Recycling the lid: Effects of subduction and stirring on boundary layer dynamics in bottom-heated planetary mantle convection. Geophys. Res. Lett. 33, L20318. http://dx.doi.org/10.1029/2006GL027668.
Tonks, W.B., Melosh, H.J., 1992. Core formation by giant impacts. Icarus 100, 326–346.
Watters, W.A., Zuber, M.T., Hager, B.H., 2009. Thermal perturbations caused by large impacts and consequences for mantle convection. J. Geophys. Res. (Planets) 114, E02,001. http://dx.doi.org/10.1029/2007JE002964.
Wilhelms, D.E., Squyres, S.W., 1984. The martian hemispheric dichotomy may be due to a giant impact. Nature 309, 138–140. http://dx.doi.org/10.1038/309138a0.
Williams, J., Nimmo, F., 2004. Thermal evolution of the martian core: Implications for an early dynamo. Geology 32, 97–100.
Yiantsios, S.G., Davis, R.H., 1990. On the buoyancy-driven motion of a drop towards a rigid surface or a deformable interface. J. Fluid Mech. 217, 547–573. http://dx.doi.org/10.1017/S0022112090000842.
Yoder, C.F., Konopliv, A.S., Yuan, D.N., Standish, E.M., Folkner, W.M., 2003. Fluid core size of Mars from detection of the solar tide. Science 300, 299–303. http://dx.doi.org/10.1126/science.1079645.
Yoshino, T., Walter, M.J., Katsura, T., 2003. Core formation in planetesimals triggered by permeable flow. Nature 422, 154–157.
Ziethe, R., Spohn, T., 2007. Two-dimensional stokes flow around a heated cylinder: A possible application for diapirs in the mantle. J. Geophys. Res. 112, 1–13.